https://doi.org/10.2352/ISSN.2470-1173.2021.5.MAAP-133

Objective evaluation of relighting models on translucent materials from multispectral RTI images

Vlado Kitanovski, Jon Yngve Hardeberg
The Norwegian Color and Visual Computing Laboratory, Department of Computer Science
NTNU – Norwegian University of Science and Technology, Gjøvik, Norway

Abstract

In this paper, we evaluate the quality of reconstruction i.e. relighting from images obtained by a newly developed multispectral reflectance transformation imaging (MS-RTI) system. The captured MS-RTI images are of objects with different translucency and color. We use the most common methods for relighting the objects: polynomial texture mapping (PTM) and hemispherical harmonics (HSH), as well as the recent discrete model decomposition (DMD). The results show that all three models can reconstruct the images of translucent materials, with the reconstruction error varying with translucency but still in the range of what has been reported for other non-translucent materials. DMD relighted images are marginally better for the most transparent objects, while HSH- and PTM- relighted images appear to be better for the opaquer objects. The estimation of the surface normals of highly translucent objects using photometric stereo is not very accurate. Utilizing the peak of the fitted angular reflectance field, the relighting models, especially PTM, can provide more accurate estimation of the surface normals.

Introduction

Reflectance Transformation Imaging (RTI) is a popular tool for the acquisition of object appearance under different directions of the light source [1]. An RTI acquisition setup is fairly simple – it requires a static camera, that is positioned orthogonally to a static object, and a light source that can be moved along a hemisphere above the object. The acquired images for each of the different light directions are used to model the per-pixel angular reflectance field i.e. the reflectance as a function of the incident light's angle. Other surface properties such as the albedo map or the surface normals of the object can be obtained from an RTI image set. These models of the object's appearance can be used in different applications, such as cultural heritage for analyzing object surface structures or their change over time [1-2] or inspection of surface anomalies [3].

The RTI imaging started with the introduction of Polynomial Texture Maps (PTM) for visualization of objects under varying illumination [4]. Using an RTI image set, a six-coefficients polynomial function is fitted to the normalized luminance intensities at each pixel, which represents the estimated angular reflectance field. This function can be used to visualize, or relight, the object under a light from an arbitrary direction. The extension to color images can be done by either fitting a separate polynomial function to each of the RGB channels, or by fitting a polynomial function to the luminance only and using constant chrominance values. Other functions have been proposed as a basis for the angular reflectance. In the context of this paper, we mention the Hemispherical Harmonics (HSH) [5] and the Discrete Modal Decomposition (DMD) [6]. Both HSH and DMD use more complex basis functions than polynomials, and therefore they have improved the relighting over PTM especially for surface points that contain higher frequencies in the angular reflectance field (such as specular highlights) [6].

Regarding the systems for RTI acquisition, the two most commonly used are free-form RTI systems - where a hand-held light source is used during acquisition together with reflecting spheres to recover the light source positions [2], and dome systems - where the positions of the light sources are fixed inside a dome and therefore the light positions are more accurate [6].

In this paper, we present the multispectral RTI system that we have developed, which uses a robotic arm for positioning the light source during the RTI acquisition. As we have identified a lack of RTI capture sets and evaluation of relighting models on translucent materials, we used our system to acquire images of materials with different translucency. We investigate the reconstruction accuracy of the relighted images as well as the surface normals estimation using the two most commonly used relighting models PTM and HSH, as well as the recent DMD. Specifically, in this paper we seek to provide answers to the following questions: Which reflectance basis is best suited for relighting translucent objects? Can the relighting models be used for estimation of the surface normals, and how? What is the influence of spectral bands on the accuracy of relighting and surface normals estimation?

Materials and Methods

Multispectral RTI System

The main components of our multispectral RTI system are the five-joints Dexter robotic arm from Haddington Dynamics [7], a turntable from Norsk Elektro Optikk [8] and the Spectral Filter Array (SFA) multispectral camera Silios CMS-C [9]. We use the robotic arm to hold the light source and move it along a virtual half-hemisphere around the object. We chose that the robotic arm should cover only half of a hemisphere in order to have larger radius (which is the distance between the object and the light source) while at the same time the robotic arm being able to cover a wide range of elevation angles for all azimuth angles of the half-hemisphere. The whole azimuth range for the light source positioning is achieved by rotating the object for 180° in the horizontal plane and around the center of the virtual hemisphere. This is done using a turntable that holds the object. During capture, the robotic arm positions the light source at the wanted measurement points on the first half-hemisphere, and after the object is rotated for 180° the robotic arm effectively positions the light source at the measurement points on the other half-hemisphere. The multispectral camera has a 3×3 SFA that captures 8 narrow bands (centered at the following wavelengths: 440 nm, 473 nm, 511 nm, 549 nm, 585 nm, 623 nm, 665 nm, and 703 nm) and one panchromatic band that is relatively constant across the whole visible wavelength range. It is positioned vertically over the turntable, with its optical axis passing very close to the center of the virtual hemisphere. As for the light source, we used a commercial LED light bulb with a luminous power of 470 lm and a color temperature of 6500K. All components are placed on a Thorlabs optical table [10] which removes ambient vibrations. The robotic arm is controlled using five variables – the angles of

each of the five joints. For each measurement position, these five angles are calculated using an iterative inverse-kinematic solver, that uses a 3D kinematic model of the robotic arm with the light source mounted. Before a capturing session, the robotic arm is manually calibrated to the reference position i.e. aligned to the 3D kinematic model. The synchronization between the robotic arm movement, the camera capture, and the turntable is achieved by controlling all of them from same programming environment. Due to the object rotation, the captured set contains two sets of images that are corrected for lens distortion and aligned in a pre-processing stage. This stage also includes spectral bands normalization using values obtained from a reference white tile, and demosaicing using bilinear interpolation. The output of the pre-processing stage is the final RTI acquisition set. A picture of our setup is shown in Figure 1. The positioning of the light source using the robotic arm is flexible in terms of azimuth and elevation angles. In this work, our multispectral RTI capture set was generated from 44 light positions that cover elevations from 15° to 65° as well as the whole azimuth range in a fairly uniform manner. We did a capture of 12 additional light positions that would be used only for evaluation of the relighting models. The unit vectors of these light positions projected on the horizontal plane are shown on Figure 2 (The 12 evaluation-only locations are shown in red). The average time for acquisition of one object (56 images) is around 6 minutes.

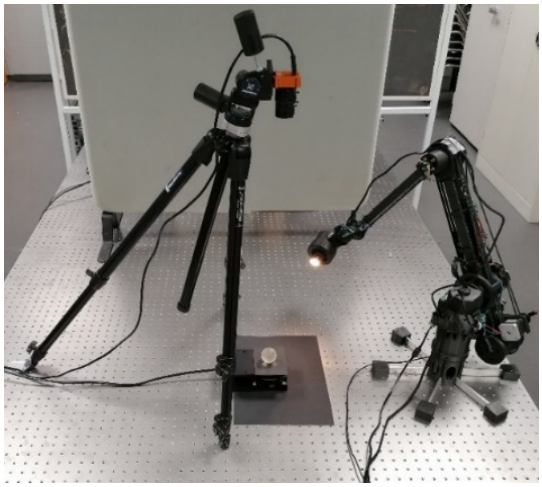

Figure 1. Our RTI system consisted of a robotic arm that holds a light source, a turntable the holds the object, and a multispectral camera

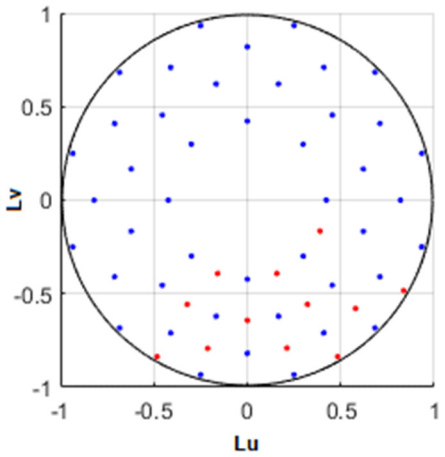

Figure 2. Light positions used in this work. The circle is the base of the virtual hemisphere, the red positions are only used for evaluation

Translucent samples

We used translucent samples from the *Plastique* collection [11]. From the three available shapes we selected only spheres as they cover broad range of surface normals. We excluded the most transparent and most opaque spheres, as well as the glossiest spheres from the collection. The nine chosen samples used in this work have different levels of translucency in terms of amount and type of volumetric scattering. They are indexed as samples from 1 to 9 and shown in Figure 3. In our work, we grouped the nine samples into different sets:

Regarding their translucency, we denote the following sets:

- Set 1 (most transparent: samples 1, 4, and 7);
- Set 2 (intermediate: samples 2, 5, and 8);
- Set 3 (most opaque: samples 3, 6, and 9).

Regarding their color, we denote the following sets:

- Set 4 (white set: samples 1, 2, and 3);
- Set 5 (amber set: samples 4, 5, and 6);
- Set 6 (blue set: samples 7, 8, and 9).

Relighting models

As previously mentioned, we evaluate the PTM [4], HSH [5], and the DMD [6] regarding their performance on relighting the translucent samples and estimating the surface normals. Each of the three models are fitted in least squares error sense on the 44 training images of each sample, for each of the nine multispectral bands separately. We used four different model parametrizations according to the number of model coefficients N: 4, 9, 16, and 25, which similarly as in [12] correspond to 1st, 2nd, 3rd and 4th degree polynomials for PTM and HSH, respectively. As for the DMD, N refers to the use of the first N modes of the discrete modal basis as a basis for the angular reflectance.

In this work we use three different approaches for estimation of the per-pixel surface normals. First, we use a classical photometric stereo (PST) based on eight relighted images from each of the three models (referred to as PST-PTM, PST-HSH, and PST-DMD). The second approach estimates the surface normals as the light direction that results in maximum luminance in the relighted image [13] (referred to as PTMmax, HSHmax, and DMDmax). In the third approach, we estimate the surface normals as the direction that bisects the angle between the maximum luminance light direction and the camera viewing direction. These are referred to as PTMmax2, HSHmax2, and DMDmax2; they are calculated using the normals from the second approach, and their calculation effectively assumes that the maximum luminance in the relighted image is due to a specular highlight.

Results

The evaluation of the relighting accuracy is performed in terms of PSNR and SSIM between the captured and the relighted images, separately for the training and for the testing images. The camera exposure time was set separately for each of the nine samples to ensure relatively good exposure across the nine bands. However, due to the variations in the spectral power distribution of the light source, the different peak sensitivities in each of the nine bands, as well as the spectrally varying properties of the samples, the resulting multispectral images had different utilization of the available dynamic range. Therefore, the captured RTI set includes images with different levels of average luminance. All of the results in this section are generated only for the pixels of the translucent surface – we effectively cropped the spheres using a circular mask on the relighted images and on the estimated surface normals.

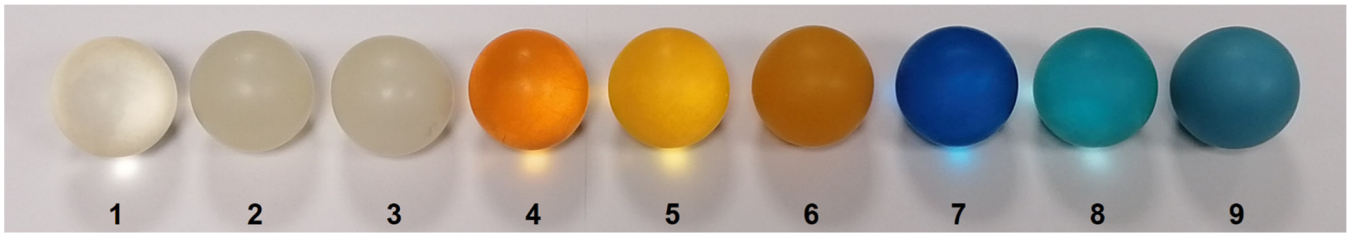

Figure 3. The nine translucent spheres from the Plastique collection [11] used in this work, from left to right indexed as 1 to 9

The relighting accuracy averaged over the 9 multispectral bands and grouped according to the level of translucency and number of model parameters is given in Table 1 and Table 2 in terms of PSNR and SSIM between the captured and relighted images. There is no big difference between using the training images (used for model fitting) and the testing images for the evaluation. As expected, using more coefficients (more basis functions) decreases the reconstruction error for all three models. Figure 4 shows a visual example of this, where an original testing image and relighted ones for the four different numbers of model coefficients. Overall, the PSNR values are relatively in the same range to what is reported for other, non-translucent, materials [12,14-15]. This means that the common relighting models may be well suited for translucent materials. It can be observed that the reconstruction becomes better as the samples become 'opaquer' – the best reconstruction is achieved for the Set 3. The images from Set 1 contained most complex highlights, which occurred both around the incident area, and on the opposite, exiting side, as the light propagated through the sample. This can be seen in Figure 5, which shows an example of images captured from the same angle for samples from the three different sets. The relatively high amount distinct specular highlights in the Set 1 may be the reason behind the DMD performing marginally better in terms of PSNR. HSH and PTM relighted images had significantly higher PSNR than DMD for the images of Set 2 and Set 3. We think that the reason behind this is the absence of a constant term in the DMD basis, because there is an offset added to many pixels in the DMD-relighted images which decreases the PSNR. This offset has lower impact on the structure captured by the SSIM metric (Table 2) which results in the DMD performing similar to PTM and HSH. As a summary, for relighting objects of higher transparency, the DMD performs marginally better than PTM and HSH both in terms of PSNR and SSIM, however, the HSH or PTM basis might be more preferable for opaquer objects. Another point is that it is more important to use more basis functions in the estimation of the angular reflectance for objects with higher transparency – so that the more complex appearance due to the light transport within the object can be represented accurately.

Figure 6 and Figure 7 show the PSNR and SSIM between the original and relighted images, averaged in a different way – across the number of model parameters and for the testing set only. The previously observed PSNR drop for DMD is mainly due to the white set (and according to Table 1, the opaquer white samples) which has strongest highlights that introduce the largest offset in the relighted image. It is interesting that PSNR is in general lower for the amber set than for the other two sets. The bluish light source could be one of the reasons, even though we don't see a clear evidence for this. Regarding the relighting of the object structure, quantified using SSIM (Figure 7), it is most accurate for the white samples. It can be seen again that there are no big differences between the three relighting models. A trend can be observed of having better relighting for the brighter images, i.e. for the mid-to-high spectral bands of the amber set, and for the lower spectral bands of the blue set. Relighting the panchromatic band has been with very good accuracy and close to the most accurately relighted spectral band.

Table 1: PSNR between the relighted images and both the training and testing images. The highest values are shown in bold

	Training images											
	4-coeff. model			9-coeff. model			16-coeff. model			25-coeff. model		
	Set 1	Set 2	Set 3	Set 1	Set 2	Set 3	Set 1	Set 2	Set 3	Set 1	Set 2	Set 3
PTM	17.60	21.50	25.35	20.87	25.44	**30.15**	23.40	28.17	33.21	26.92	31.73	36.36
HSH	17.66	**21.51**	**25.62**	**21.50**	**25.85**	29.35	23.57	**28.43**	**33.52**	27.52	**32.23**	**36.52**
DMD	**18.67**	19.64	20.96	21.42	22.67	23.46	**24.65**	26.39	27.00	**27.59**	28.74	29.60
	Testing images											
	4-coeff. model			9-coeff. model			16-coeff. model			25-coeff. model		
	Set 1	Set 2	Set 3	Set 1	Set 2	Set 3	Set 1	Set 2	Set 3	Set 1	Set 2	Set 3
PTM	17.43	**21.46**	25.40	20.52	25.31	**29.81**	22.96	27.91	32.66	25.78	30.72	34.87
HSH	17.50	21.44	**25.60**	**21.18**	**25.82**	29.36	23.21	**28.14**	**32.95**	**26.47**	**31.26**	**35.06**
DMD	**18.49**	19.49	20.74	20.94	22.38	23.44	**23.99**	26.13	27.17	25.80	27.70	29.12

Table 2: SSIM between the relighted images and both the training and testing images. The highest values are shown in bold

	Training images											
	4-coeff. model			9-coeff. model			16-coeff. model			25-coeff. model		
	Set 1	Set 2	Set 3	Set 1	Set 2	Set 3	Set 1	Set 2	Set 3	Set 1	Set 2	Set 3
PTM	0.65	**0.83**	**0.88**	**0.69**	0.85	**0.93**	0.74	0.90	**0.95**	0.82	0.94	**0.97**
HSH	0.66	**0.83**	**0.88**	**0.69**	**0.87**	0.92	0.75	0.91	**0.95**	0.82	0.94	**0.97**
DMD	**0.69**	0.82	0.83	0.68	0.85	0.90	**0.78**	**0.93**	0.93	**0.84**	**0.95**	0.95
	Testing images											
	4-coeff. model			9-coeff. model			16-coeff. model			25-coeff. model		
	Set 1	Set 2	Set 3	Set 1	Set 2	Set 3	Set 1	Set 2	Set 3	Set 1	Set 2	Set 3
PTM	0.66	0.83	0.88	**0.70**	0.86	**0.93**	0.75	0.90	**0.94**	0.81	0.93	**0.95**
HSH	0.67	**0.84**	**0.89**	0.69	**0.88**	0.92	0.75	0.90	**0.94**	**0.82**	0.93	**0.95**
DMD	**0.69**	0.82	0.84	0.69	0.85	0.90	**0.78**	**0.92**	0.92	**0.82**	0.93	0.94

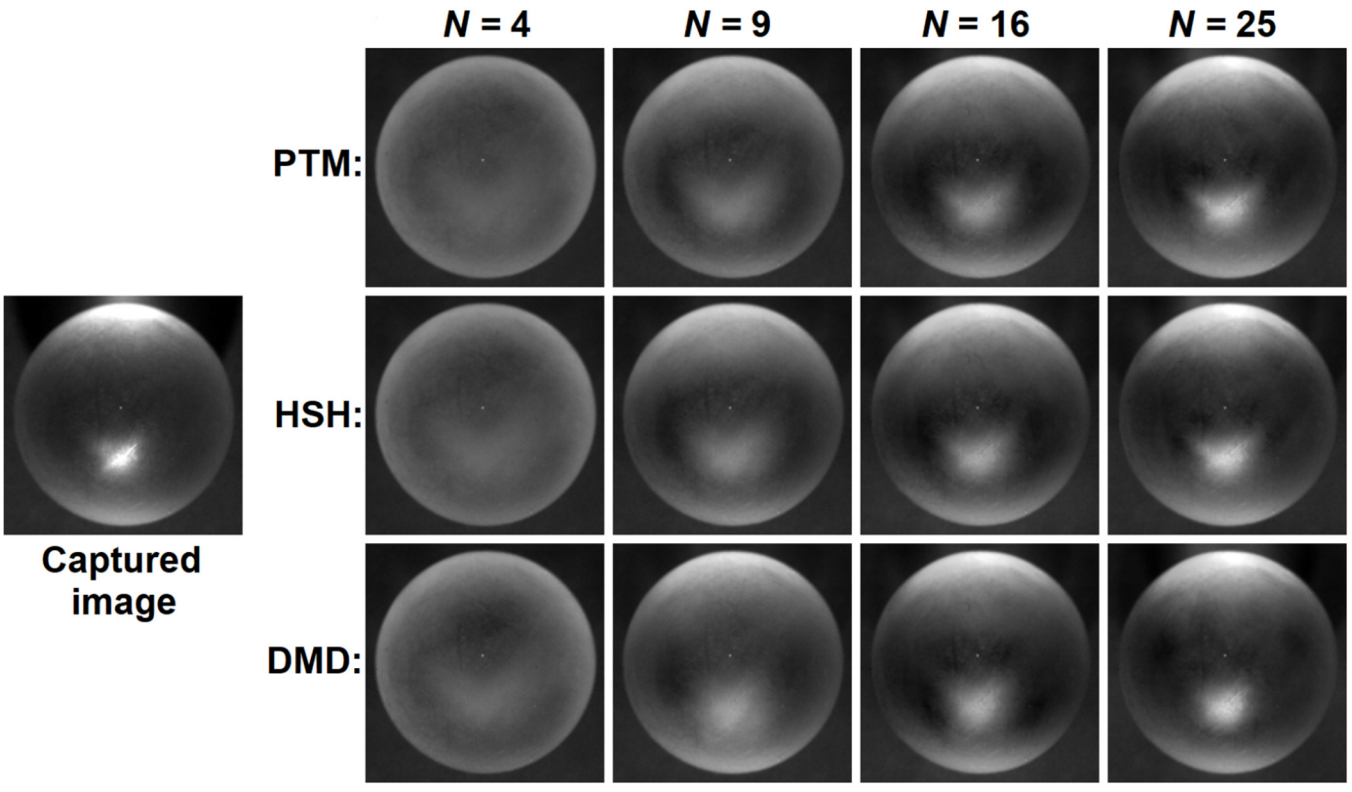

Figure 4. Relighted images using PTM, HSH, and DMD, with four different number of parameters, N. The captured image (leftmost) is from the testing set (Azimuth = -90°, Elevation = 50°) of sample 1, panchromatic band

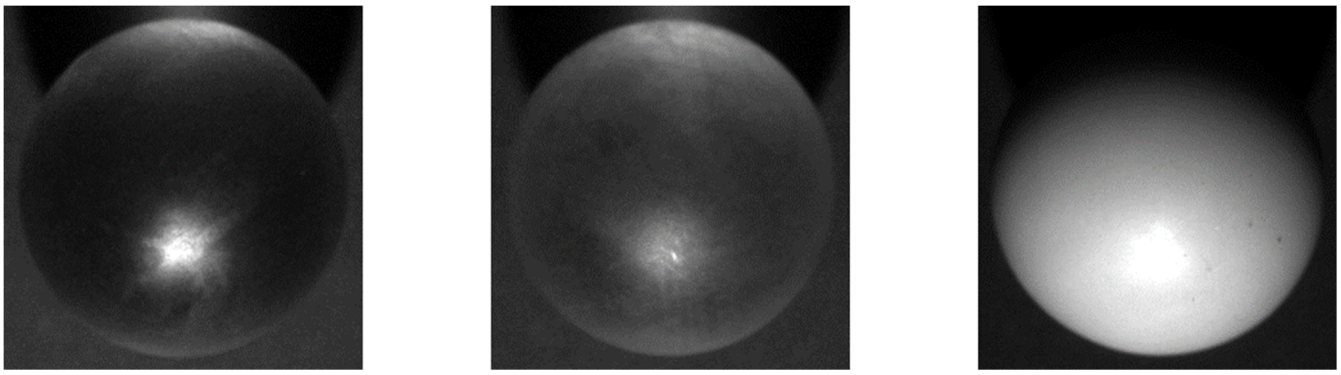

Figure 5. Captured images of band 473nm for samples 7 (left), 8 (middle), and 9 (right)

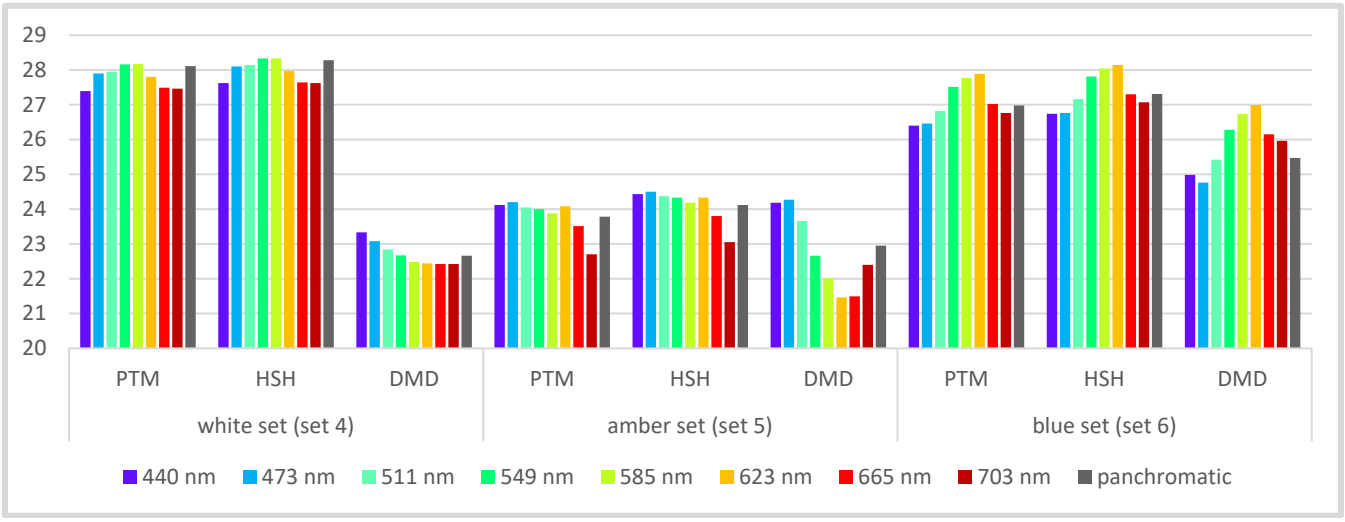

Figure 6. PSNR between the relighted images and original images, for different spectral bands and colors of the samples

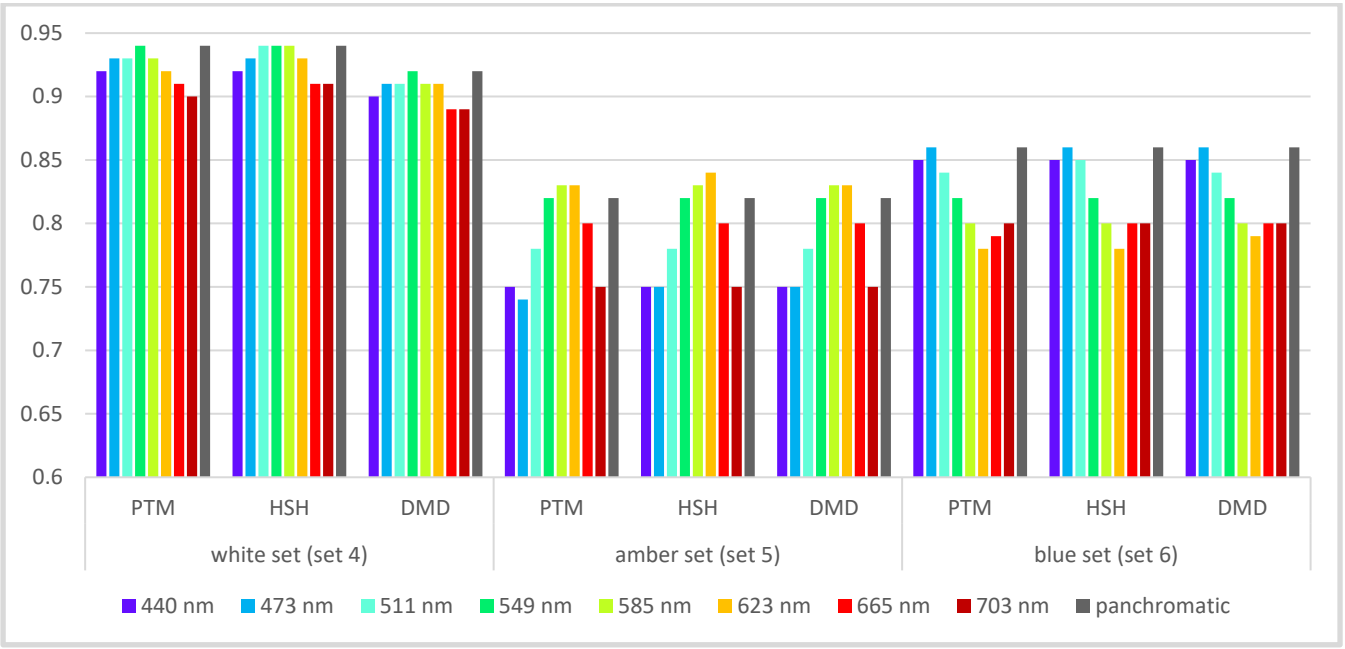

Figure 7. SSIM between the relighted images and original images, for different spectral bands and colors of the samples

The reconstruction of the surface normals using the three different approaches was evaluated in terms of the average angular error (in degrees) between the estimated and the surface normals reference. We do not have the ground-truth for the surface normals of each of the samples, so the reference used in the evaluation was a synthetic ideal sphere. There is a mismatch between the actual surface normals of the samples and the synthetic ones due to small translations and small size and shape variations in the samples, which invalidates the actual absolute numbers for the calculated angular error. However, we argue that the relative comparisons and trends observed in the calculated angular error are still valid, as after all, the mismatch between the real and the synthetic ground-truth is relatively very low.

Figure 8 shows the average angular error using the three approaches (PST-, -max, -max2) for each of the three relighting models (PTM, HSH, and DMD), averaged over the spectral bands and number of model parameters, and calculated separately on the sets grouped according to their translucency (Set 1, Set 2, and Set 3). As expected, the estimation of surface normals using PST approach is best for the opaquest Set 3, which is also the case for the other two approaches. Calculating the surface normals as the direction of maximum relighted luminance results in the largest errors for the majority of cases, even though there can be examples where it performs better than the PST approach. Calculating the surface normals as the direction that bisects the angle between the direction of maximum relighted luminance and the camera viewing direction seems to work best, especially for the PTM fits (PTMmax2). Regarding the number of model coefficients, using $N = 9$ leads to best estimation overall, while using large N can lead to larger errors. For the cases when $N = 9$, the surface normals estimation is with reversed trend between Set 1 and Set 2 – the estimation is slightly more accurate for Set 1.

Figure 9 shows the average angular error calculated separately on the sets grouped according to their color (Set 4, Set 5, and Set 6). It can also be seen that the surface normals estimation using the assumption of maximum relighted luminance due to specular highlights is better, with PTMmax2 being better than the other two. The accuracy of estimation of the surface normals appears to be different among the spectral bands. The spectral bands that are darker and therefore with higher contrast of the specular highlights – e.g. the low spectral bands of the amber set and the mid-to-high spectral bands of the blue set, lead to more accurate calculation of the surface normals.

Figure 10 shows an example of the estimated surface normals of the three blue samples (Set 6) from the panchromatic channel and with $N = 9$ coefficients in the relighting models. It shows what can be observed in general that PTMmax, HSHmax, and DMDmax make larger errors in estimating the elevation component of the surface normals. It can also be seen that the estimation of the surface normals that are closer to horizontal orientations (near the edges of the captured spheres) is with quite larger errors. This is due to the maximum relighted luminance occurring not because of specular highlights at the incident point but because of the highlights due to the scattering at the exiting point – this can be observed in Figure 4 and Figure 5. The lower ability of PTM to relight highlights can be the reason behind the better performance for reconstructing the surface normals using PTMmax2. As the performance of the surface normals estimation is specific to the size and the shape of the samples used, the better performance of PTMmax2 may not occur in general.

Conclusions

In this paper, we used a multispectral RTI capture set of objects with different translucency and color to evaluate three different reflectance bases that are used for modeling the angular reflectance field: PTM, HSH, and DMD. The evaluation was done on equal terms - for the same number of basis functions i.e. for the same number of fitted model parameters. The conclusion points of this work can be summarized into the following: 1) The commonly used angular reflectance bases can also be used to model the appearance of, and relight, translucent objects. The number of basis functions used may need to be higher for more transparent objects whose appearance under directionally varying illumination is more complex; 2) The DMD model showed marginally better relighting for the most transparent samples both in terms of PSNR and SSIM. For the opaquer samples, HSH and PTM seem to be better than DMD, especially in terms of PSNR; 3) Regarding the impact from the spectral bands, we observed that in SSIM terms, the relighting is more accurate for spectral bands where the object is more reflective and therefore, the captured image is brighter and with more details; 4) The estimation of surface normals using Lambertian-like assumptions degrades as the object becomes more transparent. Assuming that the maximum relighted luminance is due to specular highlights can lead to more accurate estimation of the surface normals; 5) There is a small difference in accuracy of the estimated surface normals between different spectral bands – spectral bands where the object is more absorptive (but specular highlights are still present) lead to more accurate estimation of the surface normals.

These conclusion points are limited to our choice of samples in this study – e.g. in terms of shape, size, color, or glossiness. While they might be within the reasonable expectations, they should be confirmed in a future and broader study.

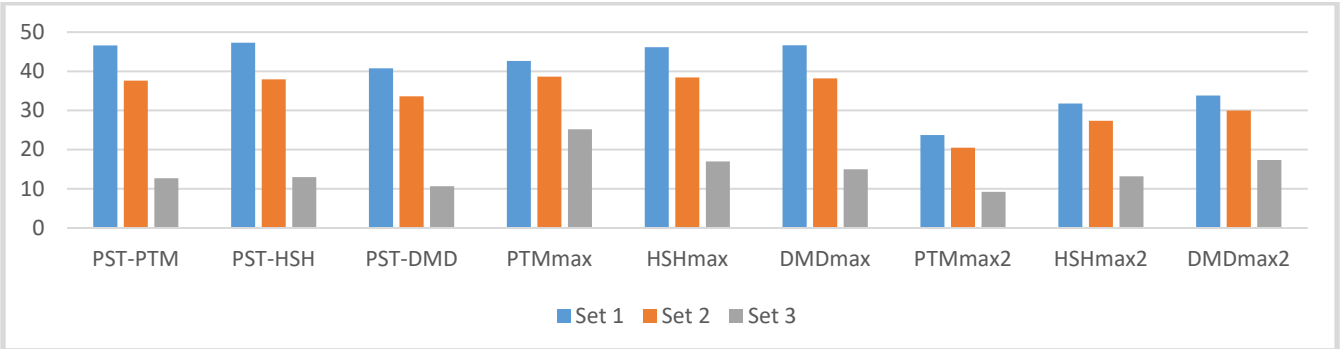

Figure 8. Average angular error (°) in the surface normals estimation for the different approaches, and according to the sample sets with different translucency

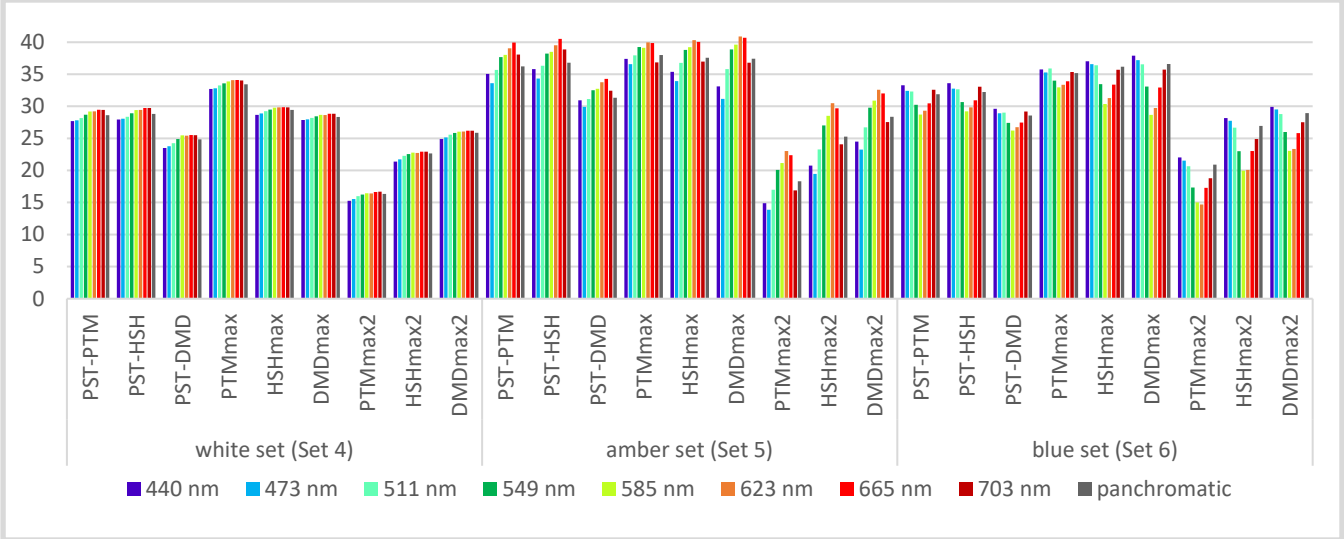

Figure 9. Average angular error (°) in the surface normals estimation for the different approaches, for different spectral bands and color of the samples

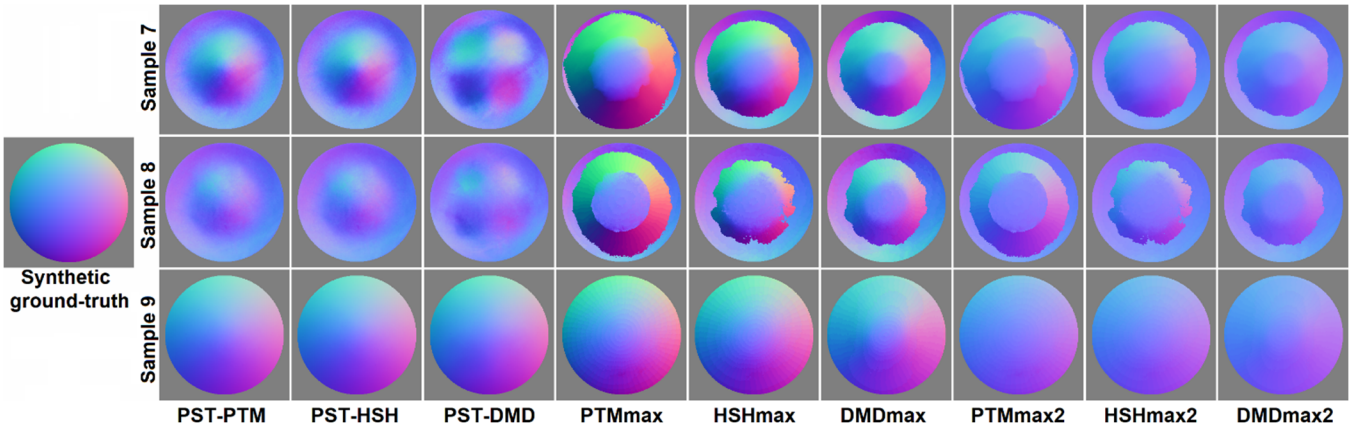

Figure 10. Estimated surface normals using the different approaches for the three blue samples. The synthetic ground-truth is shown leftmost

References

[1] Reflectance Transformation Imaging (RTI), Available online: http://culturalheritageimaging.org/Technologies/RTI

[2] I. Ciortan, R. Pintus, G. Marchioro, C. Daffara, and A. Giachetti, "A practical reflectance transformation imaging pipeline for surface characterization in cultural heritage,", EUROGRAPHICS Workshop on Graphics and Cultural Heritage, 2016.

[3] G. Pitard, G. Le Goic, A. Mansouri, H. Favreliere, M. Pillet, S. George, and J. Y. Hardeberg, "Robust Anomaly Detection Using Reflectance Transformation Imaging for Surface Quality Inspection," Scandinavian Conference on Image Analysis : Image Analysis, vol. 10269, no. 1, pp. 550–561, Jun. 2017.

[4] T. Malzbender,, D. Gelb, and H. Wolters. "Polynomial Texture Maps", Proc. ACM SIGGRAPH, 28, 519-528, 2001.

[5] P. Gautron, J. Krivanek, S. N. Pattanaik, and K. Bouatouch, "A Novel Hemispherical Basis for Accurate and Efficient Rendering," Eurographics Symposium on Rendering 2004, pp. 1–10, 2004.

[6] G. Pitard, G. Le Goic, A. Mansouri, H. Favreliere, S.-F. Désage, S. Samper, and M. Pillet, "Discrete Modal Decomposition: a new approach for the reflectance modeling and rendering of real surfaces," Machine Vision and Applications, vol. 28, no. 5-6, pp. 607–621, Jul. 2017.

[7] Haddington Dynamics, online. https://www.hdrobotic.com/

[8] Standard Rotation Stage, online. https://www.hyspex.com/hyspex-products/accessories/tripods-and-stages/rotation-stages/#stdRot

[9] Silios multispectral cameras, online. https://www.silios.com/cms-series

[10] Optical breadboards, online. https://www.thorlabs.com/newgrouppage9.cfm?objectgroup_id=7159

[11] J-B. Thomas, A. Deniel, and J. Y. Hardeberg, "The Plastique collection: A set of resin objects for material appearance research", Proc. 14th Conferenza del colore, pp. 1-12, 2018.

[12] M. Zhang and M. S. Drew, "Efficient robust image interpolation and surface properties using polynomial texture mapping", EURASIP Journal on Image and Video Processing, 25, 2014.

[13] L. MacDonald and S. Robson, "Polynomial Texture Mapping and 3D Representations", Proc. International Archives of Photogrammetry, Remote Sensing and Spatial Information Sciences, Vol. XXXVIII, Part 5, 2010.

[14] R. Pintus, T. Dulecha, A. Jaspe, I. Ciortan, and E. Gobbetti, "Objective and Subjective Evaluation of Virtual Relighting from Reflectance Transformation Imaging Data", EUROGRAPHICS Workshop on Graphics and Cultural Heritage, 2018.

[15] A. Zendagui, J-B. Thomas, G. Le Goic, Y. Castro, M. Nurit, A. Mansouri, and M. Pedersen, "Quality assessment of reconstruction and relighting from RTI images: application to manufactured surfaces", Proc. 15th International Conference on Signal-Image Technology & Internet-Based Systems (SITIS), 2019.

JOIN US AT THE NEXT EI!

IS&T International Symposium on

Electronic Imaging

SCIENCE AND TECHNOLOGY

Imaging across applications . . . Where industry and academia meet!

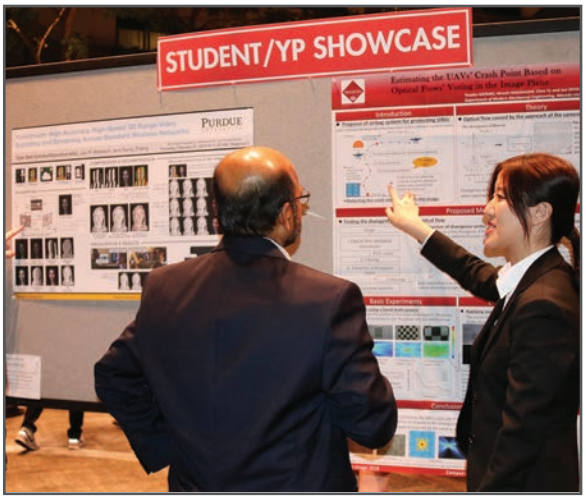

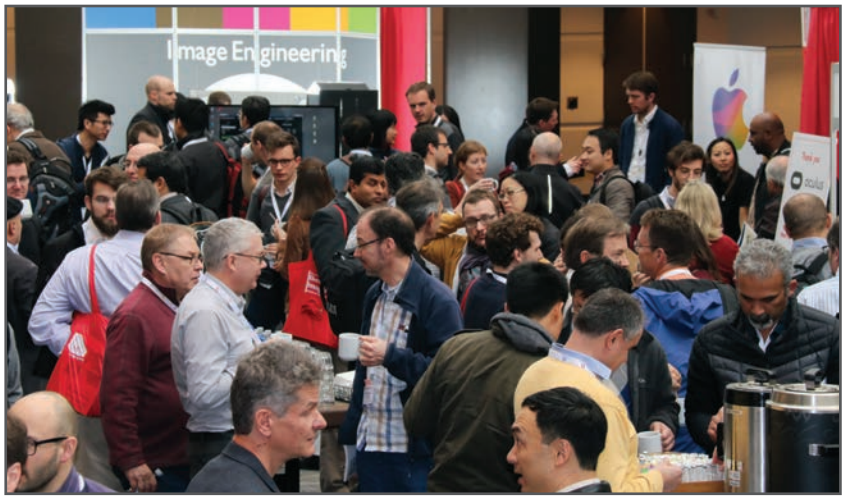

• SHORT COURSES • EXHIBITS • DEMONSTRATION SESSION • PLENARY TALKS •
• INTERACTIVE PAPER SESSION • SPECIAL EVENTS • TECHNICAL SESSIONS •

www.electronicimaging.org

IS&T
imaging.org